Rapid Optical Detection and Classification of Microbes in Suspicious Powders

W. F. Hug*[a], R. Bhartia[b], K. Sijapati[a], Q. Nguyen[a], P. Oswal[a], and R.D. Reid[a]

[a] Photon Systems, Inc., 1512 Industrial Park St., Covina, CA 91722
[b] Jet Propulsion Laboratory/Caltech, 4800 Oak Grove Dr., Pasadena, CA 91109

Abstract

This paper describes a rapid, reagentless, standoff method of detection & classification of bulk and trace suspicious substances on natural surfaces using solar-blind deep UV excitation and detection. Detection is typically accomplished in less one second. The detection method is solar blind and can be employed at standoff distances up to 5 m or more without interference from natural or man-made light sources.

By this method, unknown suspicious powders, that potentially contain biological hazards, are automatically triaged using a four-step sequential iteration of Principal Component Analysis methods using pre-determined eigenvector sets to: 1) detect and differentiate whether a sample is bio or non-bio; 2) whether the detected bio is microbial, protein, or plant; 3) if microbial, whether the sample is a bacterial cell or spore, yeast, fungi, or fungal spore; and 4) to provide some higher level of cellular differentiability. The same method is also applicable to a wide range of chemical agents and explosives materials.

The method and related instruments employ sample excitation at 248.6 nm and detection over a spectral range from 250 nm to below 350 nm, a spectral region blind to solar and most man-made light sources. Detection and classification is accomplished in less a few seconds. Sample detection and classification rates can be over 20 per second. Fully integrated and self-contained hand-held instruments are presently under development with an overall weight less than about 8 lbs, including a battery for over 8 hours of typical use. The standoff detection range is nominally 5 cm to 5 m.

Keywords: deep UV Raman; native fluorescence; chemical; biological; explosives; detection; classification; standoff; handheld.

1. INTRODUCTION

The goal of this paper is to demonstrate the ability of deep UV optical methods to detect and classify trace levels of suspicious powers on surfaces with a focus on detection of microbial powders. This paper is an extension of a prior paper [1]: *Hug, W.F., Bhartia, R., K. Sijapati, L.W. Beegle, and R.D. Reid, "Improved sensing using simultaneous deep UV Raman and fluorescence detection-II", SPIE Security & Defense, Vol. 9073, No. 20, May 7, 2014*. This prior paper provides much of the background on deep UV Raman and fluorescence detection methods employed in this present paper.

Since the earliest days of laser-based Raman spectroscopy, it has been known that even a small amount of fluorescence generated within a targeted material or other material encompassed by the laser beam spot on the target can interfere with or obscure Raman emissions. This is because Raman cross-sections are typically in the range of 10^6 to 10^8 times weaker than fluorescence. More recently, but still over 35 years ago, Asher [2] [3] showed that fluorescence from natural materials do not fluorescence below about 270 nm, independent of excitation wavelength. Some synthetic semiconductor materials can be made to emit at shorter wavelengths, but not natural materials. The materials that emit at wavelengths between 270 nm and 340 nm are single ring organics and their variants, as well as biological material, including microbes and their building blocks: aromatic amino acids, peptides, and proteins. Above about 340 nm fluorescence occurs from multi-ring organic materials and their variants. Therefore, to create a fluorescence-free spectral region between the excitation and Raman emission wavelengths up to about 3600 cm-1, excitation needs to be below 250 nm. Another important aspect of excitation below 250 nm is the fact that fluorescence spectra can be altered by strong OH stretch Raman bands of water if excitation occurs at longer wavelengths, where Raman and fluorescence emission spectral regions overlap. This can interfere with and alter fluorescence emission spectra of low ring organics and biological material. This is not the case for lasers that provide excitation at longer wavelengths, although excitation above 1 µm produces reduced fluorescence backgrounds, but also produces very poor sensitivity. In the case of deep UV excitation, fluorescence is important since it adds significant information to assist in sample identification.

2. DEEP UV MICROBIAL DETECTION

There are many important needs for rapid, reagentless, standoff or non-contact microbial detection and identification to enable effective response to a bioterrorism event, to avoid spreading of suspicious powders, or to enable rapid adjustments to physical therapies using antimicrobials in the case of wound therapy or other infection events. The most advanced present methods using polymerase chain reaction (PCR) takes hours to perform, and culturing methods takes days to perform. Both method require sample extraction and processing, a high level of skills, and costly reagents and disposable materials. Because of the intimate contact with a sample, there is also high risk of accidental spreading of the hazardous material, especially if it has been weaponized.

Following is a description of a method to detect and roughly characterize suspicious powders on surfaces, with a focus on microbial powders. Detection and classification time is much less than 1 s, with detection/classification events repeated at up to about 20 per second. The method can be accomplished at non-contact standoff distances from 5 cm to 5 m using a hand-held sensor weight in the range of 4 lbs to 8 lbs, depending on the standoff distance. This basic subject is being studied at many organizations with several references provided here: [4] through [16]. This deep UV standoff method is not destructive and allows for subsequent testing using PCR or other methods for higher levels of identification.

Microbes include a wide array of living material with a wide array of sizes and characteristics including bacteria, yeast, algae, fungi, viruses, etc. Common to all these living materials is their fundamental makeup of nucleic and amino acids. Nucleic acids and carbohydrates each account typically between 2% and 15% of the dry weight of a microbe. The dry weight of protein comprises between 40% and 60% of the dry weight of microbes [17]. Fundamental building blocks of protein are the aromatic amino acids, tryptophan, tyrosine, and phenylalanine, all of which are highly fluorescent. Other cellular materials such as DNA, lipids, membranes, and saccharides are essentially non-fluorescent. If these materials or the other amino acids were fluorescent, fluorescence emission from proteins would be much more complex. Fortunately, the fluorescence characteristic of microbial material is vastly dominated by the three aromatic amino acids, which form a large variety of proteins and protein conformations to create unique fluorescence signatures to enable spectroscopic differentiability of microbes. Although DNA itself has little fluorescence signature, it codes for proteins which do have significant fluorescence emission and are related to DNA through this coding.

Below, in Fig. 1a, is an excitation-emission matrix (EEM) diagram of a Bacillus subtilis vegetative cell. The EEM diagram show the relationship between excitation wavelength, emission wavelength, and fluorescence intensity, represented as iso-intensity contours in the EEM diagram. The two different fluorophors shown with excitation maxima about 280 nm and 225 nm are the primary fluorophors which are made up of the composite emissions of the three aromatic amino acid residues in this cell. Shown also are the Rayleigh scatter line, where emission and excitation wavelength are equal. The secondary diagonal line is the 2nd order spectrum of the Rayleigh scattering, an artifact of the spectrofluorimeter spectrometer. Figure 1b show the molar absorptivity of the three aromatic amino acids with the excitation axes co-aligned with the EEM diagram.

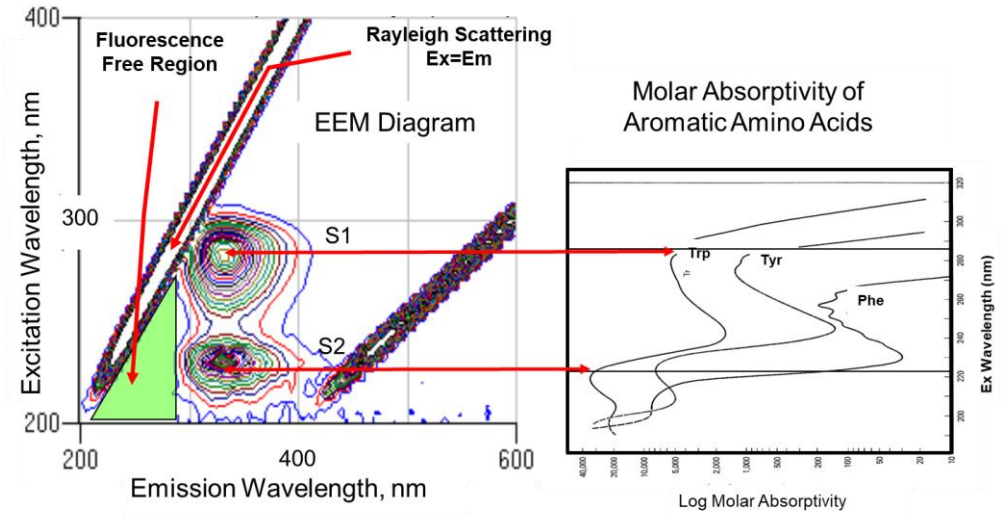

Figure 1. EEM diagram of B. subtilis vegetative cell correlated with molar absorptivity spectrum of amino acids

Below, in Fig. 2, are high resolution fluorescence spectra showing the variation in the leading edge of the fluorescence emission signature of 3 bacteria and one yeast microbes: B. subtilis (44 GC%), E. coli (51 GC%), P. aruginosa (64 GC%), and S. cereviciae (38 GC%, Y). The reference to GC% (or G+C%) above is the guanine plus cytosine content of a microbe, in percent. Four bacteria are shown in Fig. 2 where the shortest emission wavelength curve is related to bacteria with the lowest Trp/Tyr ratio and lowest GC%, B. subtilus. Wavelength increases with Trp/Tyr ratio and increasing GC%. This is an indication of a relationship between Trp/Tyr ratio and GC% content. The exception is the yeast, S. cereviciae. Note that there are no Raman emissions evident from this concentration of microbes in the 250 nm to 275 nm spectral range corresponding to 0 to 4000 cm-1 in Raman shift. Only fluorescence emissions are detectable.

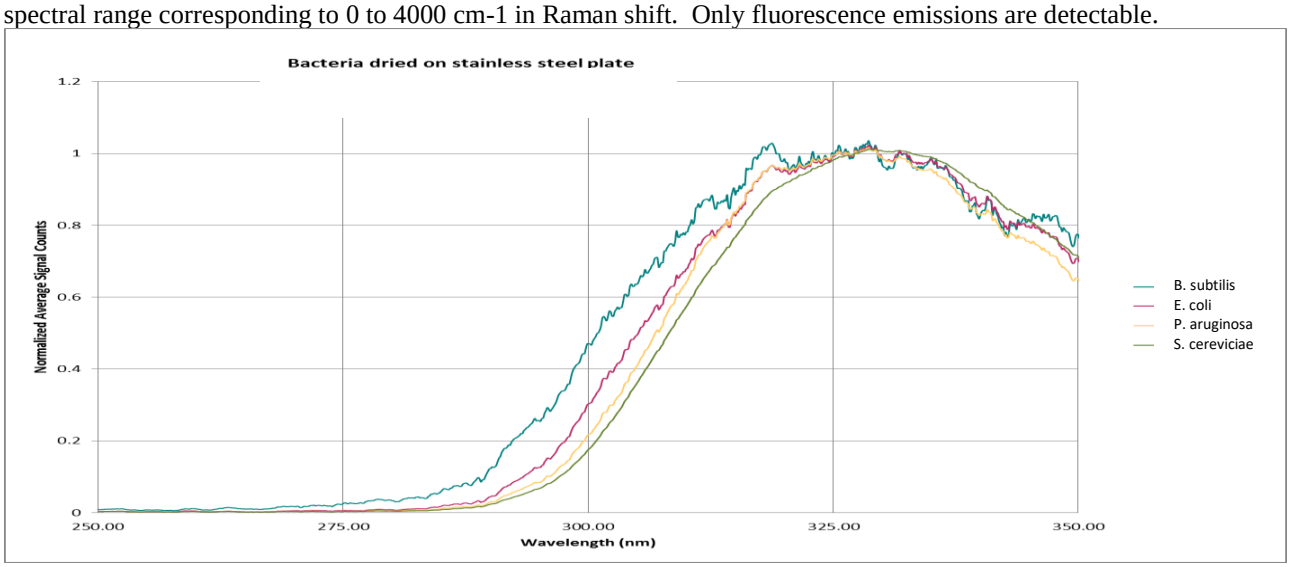

Figure 2. Native fluorescence spectra of microbes of different GC% content. 248 nm excitation.

Below in Fig. 3 is the dark subtracted and normalized fluorescence spectra of Tyr, Trp, and six (6) microbes, showing only the spectral region from 282 nm to 315 nm. The ordinate is restricted to show only the region around the 50% normalized intensity value between 44% and 56% to enable a clearer view of the spectral differences between microbes.

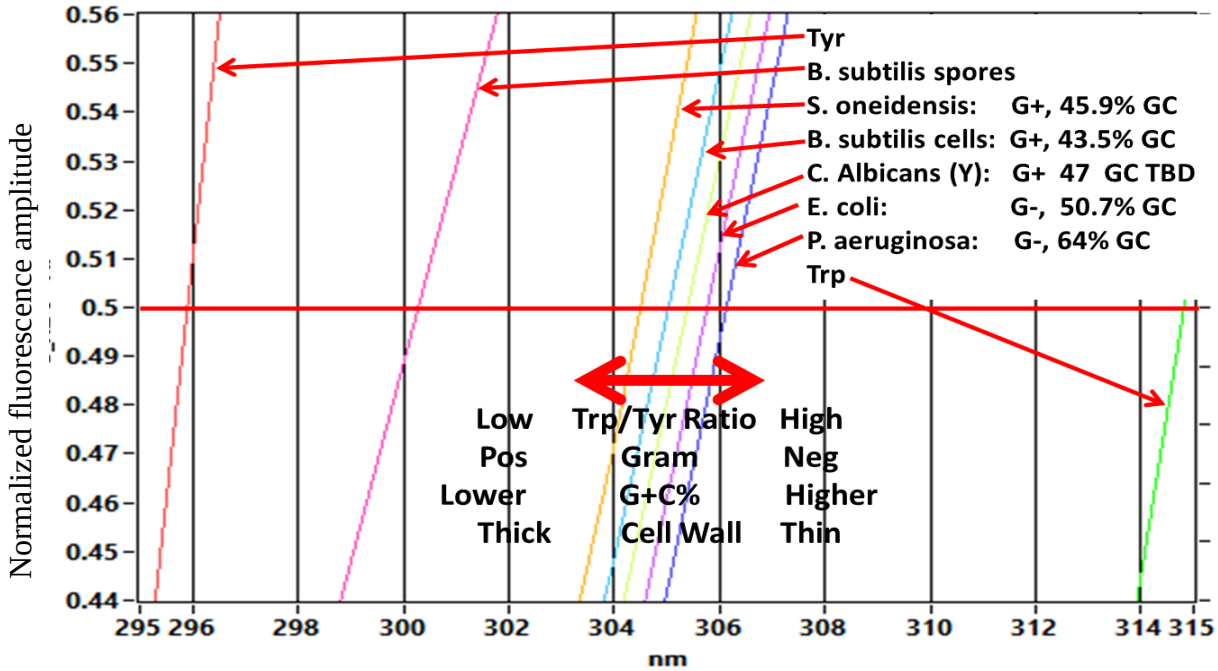

Figure 3. Normalized native fluorescence of 6 microbes plus Trp and Tyr in a narrow spectral and amplitude range.

Figure 3 also shows various trends for microbes based on the trends for Trp/Tyr ratio, based on the wavelength, measured at the 50% normalized fluorescence emission point, of various microbes compared to the corresponding wavelengths for Trp and Tyr. Since the cell wall of spores is dominated by dityrosine, they are closer to the Tyr curve than Trp. Vegetative cells have a larger fractional content of Trp. The Gram polarity of cells is also related to Trp/Tyr content, where Gram negative cells tend to have more Trp and Gram-positive cells have more Tyr. The GC% content of cells also trends with Trp/Tyr ratio, with vegetative cells having more GC% content than spores. Similarly, the thickness of cell walls is lower for vegetative cells with higher Trp content and thinner for spores or spore formers.

It is known that the GC% content of bacteria covers a wide range from about 25% to 75% and show very little intergenomic variability such that within-species variability is low, and polymorphism can be neglected [18]. One of the methods to determine the relationship and statistical variability of the relationship between GC % and Trp/Tyr ratio % is to measure the wavelength of the 50% blue wing fluorescence wavelength of different microbes. Table I below shows the Trp/Tyr ratio as determined from the blue wing fluorescence for the eight (8) organism shown. Also shown in Table I is the virulence of the various organisms including the some of the organisms of most concern for terrorism including: B. anthrasis, Y. pestis, V. choloerae, and B. pseudomallei.

Table I. Bacterial species listed in order of G+C% content along with Trp/Tyr fluorescence ratio.

Organism	GC Mole%	Trp/Tyr FL %	Gram	Spore	Virulence
Clostridium botulinum	28.2/24.8?		P	X	2
Rickettsia prowaseki	28.9		N		3
Staphyloccoccus aureus	32.8		P		2
Bacillus cereus	32	60.8	P	X	1
Candida albicans (Y)	33.5	50			
Enterococcus faecalis	34-36,37.5		N		1
Staphyloccoccus simulans	34-38		P		1
Bacillus antracis Ames	35.2		P	X	2
Streptococcus agalactiae	35.5		P		1
Bacillus thuringiensis	35.7				
Proteus vulgaris	36-40				1
Bacillus magaterium	37	57.4	P	X	1
Streptococcus pyogenes	37.7				
Saccharomyces cereviciae (Y)	38				
Proteus mirabilis	39.5		N		1
Bacillus subtilis	44.1	47.6	P	X	1
Acinetobacter calcoaceticus	42		N		2
Schewanella oneidensis MR1	45.9	45.5	N		1
Yersinia pestis	47.6		N		3
Vibrio cholerae	47.6		N		3
Escherichia coli	50.7	51.9	N		2
Shigella dysenteriae	50		N		2
Samonella tphi	52.1		N		2
Enterobacter aerogenes	54.3		N		1
Alcaligenes faecalis	57	62 – 63.5	N		1
Enterobacter cloacae	57.2		N		1

Aeromonas hydraphila	55.7		N		1
Brucells suis 1330	57.2		N		3
Brucella melitensis	57.2		N		3
Aeromonas hydraphila	59-62		N		1
Pseudomonas putida	61.4		N		1
Pseudomonas aeruqinosa	64	54.5	N		1
Mycobacterium tuberculosis	65				
Micrococcus luteus	66.3		P		1
Burkholderia pseudomallei	68.06		N		3

Below, in Fig. 4 is a plot of GC% content and Trp/Tyr% of eight (8) different organisms ordered on the x-axis in order of GC% content. The relationship between GC% and Trp/Tyr% is clearly not equal, although it is nearly equal between GC% from about 44% to 64%. However, there are major deviations between a GC% of 32% and 40%. Although GC codes for fluorescent proteins, the relationship between Trp/Tyr% and GC% is very complicated. The results in Fig. 4 are purely phenomenological with no known mechanism. Although this view of the relationship of Trp/Tyr% to microbial classification may not follow easy explanation, Figure 5 below and the triaging analysis following provides more hope of correlating fluorescence properties to microbial classification.

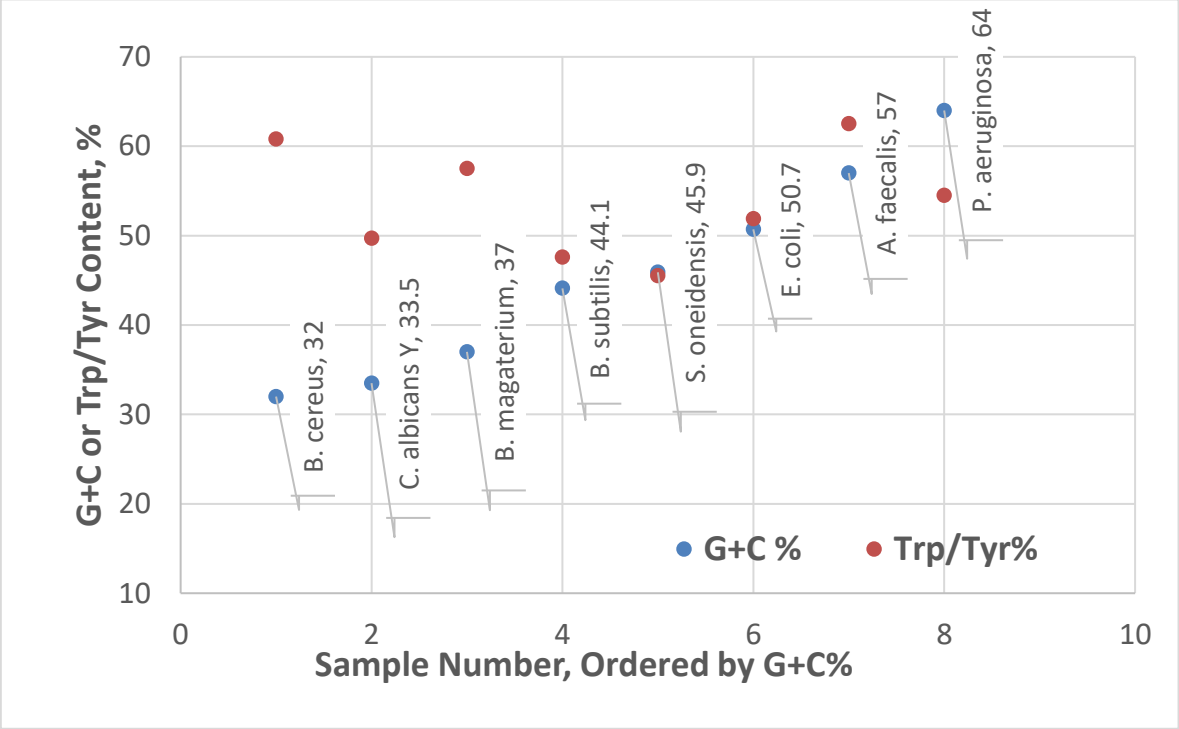

Figure 4. Relationship between G+C% and Trp/Tyr% of several microbes

Another illustration of the native fluorescence spectroscopic relationship to microbial classification is shown in Fig. 5 below, taken with a Photon Systems deep UV native fluorescence microscope called Micro-MOSAIC. The relationship between GC% content and microbial deep UV fluorescence was previously illustrated in the deep UV epifluorescence chemical image, taken in 6 spectral bands from 280 nm to 380 nm with excitation at 224 nm, shown below in Fig. 5. Color in this figure is NOT arbitrary but is related to the amplitude of signal in the first three principal component axes of the multi-variate analysis method, Principal Component Analysis (PCA), where the amplitude of PC1, 2, and 3 axes are proportional to the amount of red, green, and blue in the image in Fig. 5. Note that the color of bacterial cells varies from yellow to green in different shades proportional to the GC% content. The spore is colored red, based on its high Tyr content.

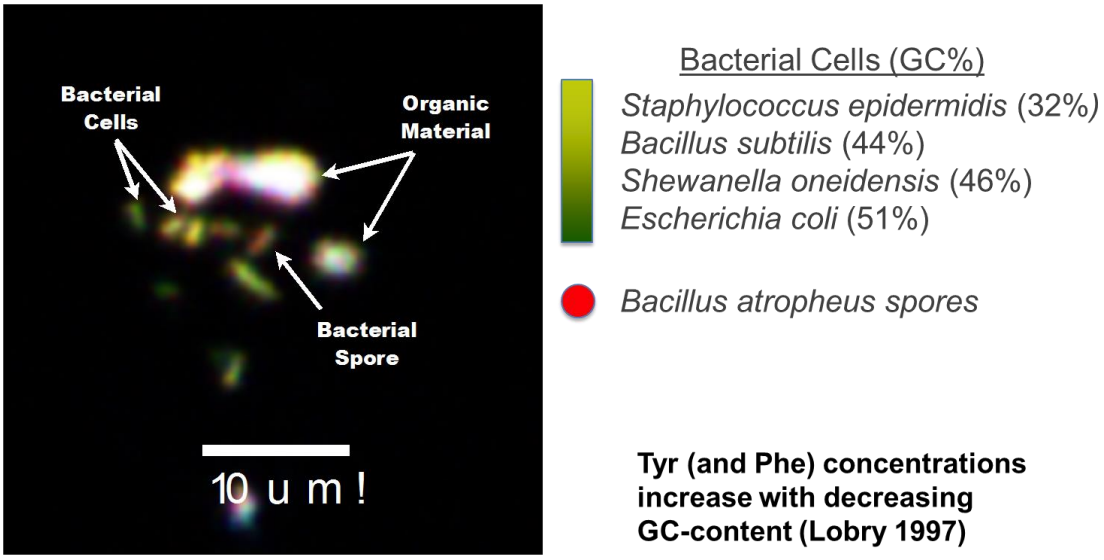

Figure 5. Six band multispectral microscopic epifluorescence image of several bacteria

To enable greater microbial differentiability, we used higher spectral resolution native fluorescence data in a process we call sequential PCA analysis to triage an unknown sample. The relative concentrations of the key aromatic amino acids and their conformation and distribution within cells are the drivers for a process of triaging samples to provide higher and higher levels of sample differentiability & characterization enabled by each subsequent real-time analysis. We demonstrated that high-resolution deep UV fluorescence spectroscopy alone can differentiate benign suspicious powders from microbes and determine which types of microbes are present. The presented analyses use spectral data that include: 1) pure microbes dried on a surface; 2) microbes mixed into an inorganic (Talc) up to 70,000:1 of inorganic to microbes by mass, i.e. < 5 microbes in laser beam spot); and 3) potential interferent or confusant materials such as other inorganic and organic powders that are non-hazardous but may be used in a hoax, and 4) other materials of potential interest.

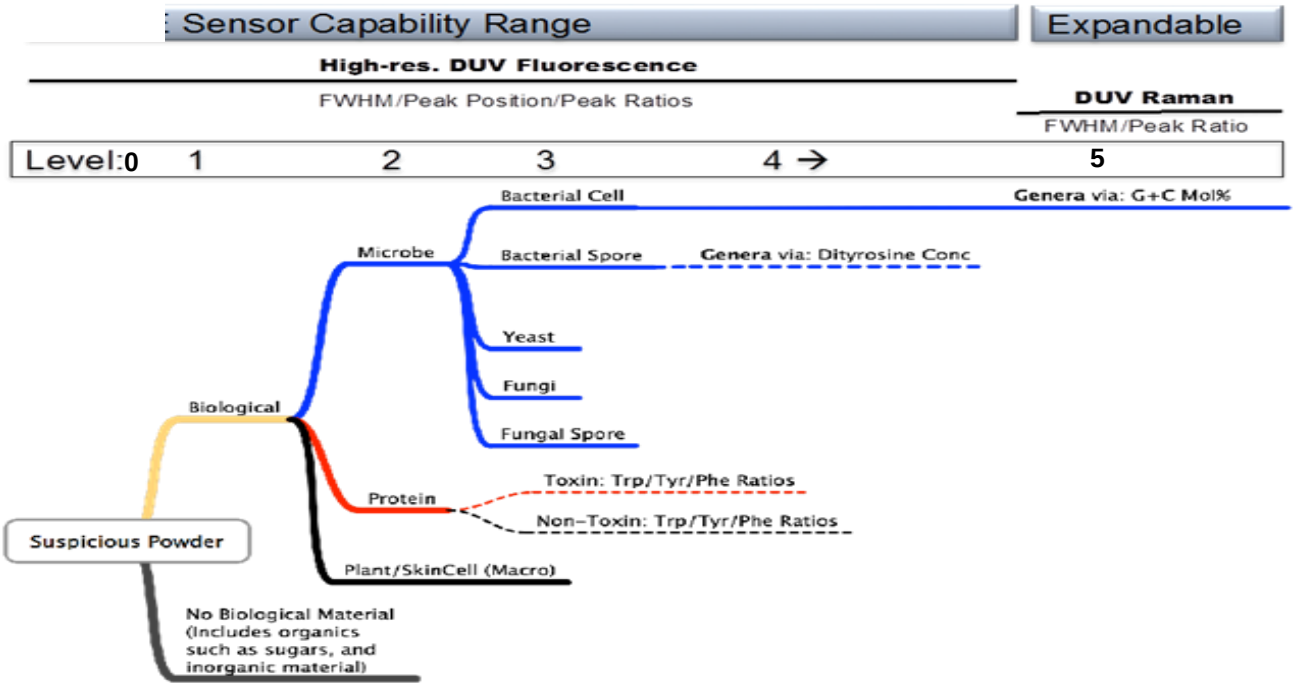

Figure 6. Graphic representation of Level 0 – 5 sample sequential triaging capabilities of deep UV fluorescence sensor.

For various experiments, we selected several microorganisms that were used to test various portions of our sample triaging method, several of which we have used throughout this project. These samples were chosen specifically for their capability for pathogenicity, or as a simulant for potentially threatening organism, however, they also each have unique physiognomies, which affect their metabolism and thus might contribute to their fluorescence spectral characteristics and subsequent position on the PCA plot. The characteristics of our chosen microorganisms are shown in Table II. Then note next to each microbe indicates whether it is a bacillus (B) or yeast (Y) and whether it was Gram-positive (GP) or Gram-negative (GN), and the GC% content of the microbe. Other materials are, for this evaluation, interferent or confusant materials categorized into a variety of pollens, protein, inorganic and organic powders, and explosives. Extreme care was taken to ensure that all materials were what is represented, and microbes were vetted to be pure and well washed of media.

Table II: Table of chemical, biological, and explosives (CBE) materials tested

Biological/Microbial Materials
B. cereus (B) GP GC32
B. megateriusm (B) GP GC37
B. subtilis (B) GP GC44
S. oneidensis (B) GN GC46
E. coli (B) GN GC51
P. aruginosa (B) GN GC64
M. luteus (B) G variable GC66
A. faecalis (B) GN GC69
S. cereviciae (Y)
Candida albicans (Y)
Pollen
Sorghum halepense (grass)
Poa pratensis (grass)
Populus tremuloides (tree/shrub)
Juniperus scopulorum (tree/shrub)
Kochia scoparia (weed)
Artemisia tridentata (weed)
Protein
lysozyme
Albumin

Inorganic Materials
Arizona road dust
augite
quartz (coarse, fine, xtal)
rhodochrosite (powd, xtal)
talc
borates,
calcite
carbonate, Ca, Mg, Na
nitrates
chlorates
perchlorates
Organic Powders
aspirin
baking powder
baking soda
corn starch
flour
fruit pectin
ammonium sulfate
anthracene
bakers yeast

Organic Powders
biphenyl
gelatine
granulated sugar
perylene
phenanthrene
powdered sugar
produce protector
pyrene
serine
glycine
histidine
proline
phenylalanine
tyrosine
tryptophan
naphthalene
Explosives
SEMTEX
C4
PETN
TNT
RDX

The sensor used for the 4-level analysis measurements is called a Biological Reconnaissance & Analysis using Non-contact Emission (BRANE 1.0) sensor, shown below in Fig. 7. BRANE 1.0 is a self-contained sensor with a 248 nm laser, laser control electronics, a 200 mm focal length spectrometer, and a 32-channel PMT array detector with multi-channel boxcar integrator and average. Spectral dispersion was 3.3 nm/pixel. This sensor weights about 9 lbs including battery. Data processing was performed with an external notebook or tablet computer. This sensor was not equipped to measure Raman, but a successor sensor is, as described in the next section.

Figure 7. BRANE 1.0 deep UV native fluorescence sensor

Level 0 Analysis

Level 0 is the first stage of sample analysis triage that provides the first, gross, evaluation of the class of a suspicious powder being addressed. At Level 0, the sensor determines whether the suspicious powder is close enough to a biological material to warrant a more in-depth analysis. At Level 0, the deep UV native fluorescence sensor can also determine if a suspicious powder is a benign material, or whether it has a signature closer to a chemical or explosive material. For Level 0 sample triage, the PCA program was trained using fluorescence spectra from all the materials listed in Table II. The spectra were background subtracted and normalized, prior to calculating the first PCA eigenvector training set, the Level Zero set. The results, shown only in 2D PCA, are illustrated in Fig. 7, where the White Powders are mostly organic and inorganic powders listed in Table II. VOCs are volatile organic compounds. AAs are aromatic amino acids. Biologicals (microbial material) and pollens are as described in Table II.

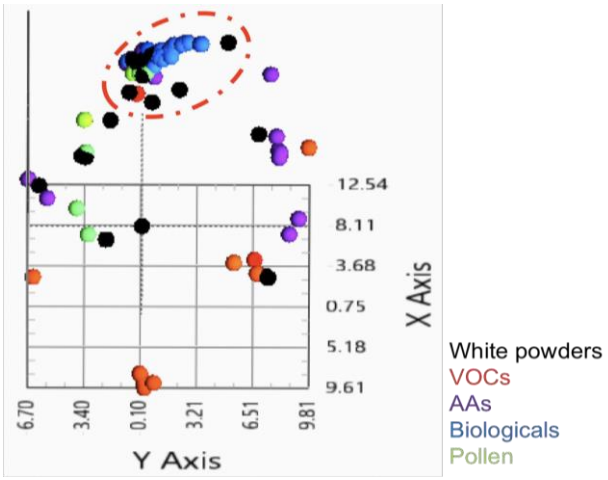

Figure 7. Level 0 triage -preliminary sample evaluation, Ex = 248 nm

This first training set is effectively evaluating the unknown sample against the broadest possible range of material to determine an approximate or preliminary classification, where an unknown is compared, using Euclidian distance in PCA space, to all knowns in the Zero library.

As shown in Fig. 7, for this first Level, microbial materials appear to cluster with other, non-microbial, materials that appear to be too close to separate. This group is circled in red in Fig. 7. In three or more dimensions, microbial separation is clearer than is possible to illustrate in the 2D image of Fig. 7, as described below.

Level 1 Analysis

The next level of triage, Level 1, of the unknown sample uses a more focused training set, the Level One set, which surrounds a smaller region of the larger, Zero PCA space, which now looks at materials in close chemometric proximity to biological material. Level 1 triage focuses on the ability of the deep UV native fluorescence sensor to differentiate biological from non-biological material. Biological materials are defined here to include microbes, proteins, as well as plant and skin cells. Non-biological materials include a long list of organic and inorganic materials that are potential interferents and confusants during these measurements, as listed in Table II.

This is the lowest level of analysis in Fig. 6 for the BRANE sensor. While details of calculations for PCA are outside the scope of this paper, the basic premise is that PCA re-represents the spectra in terms of Principal Components (PC). Each PC states a weighting for each spectral bin (pixel), which are applied to each spectrum in the input dataset and summed to provide a single value for a PC. Weights for each PC are determined by the algorithm and are dependent on the variance of the input dataset, i.e., if the dataset changes, and that change increases or decreases the variance in the data, the weights for each PC will change. The PCs, when output, are ranked in order of the weightings that accentuate the spectral regions that have the greatest variance. However, it is not necessarily the first PC should be used – the choice of PCs to use requires analysis of the weights to ensure that they are not accentuating instrument artifacts or other non-chemical related features.

It should be noted, however, that an unknown can be compared to a fixed library data set without altering training set weights. In that way, the PCA space is an invariant chemometric space in which to compare the location of the unknown compared to the knowns in the library set. It should also be noted that different library training set weights can be calculated that "zoom" into a selected smaller region of the broader PCA chemometric space that enables further differentiation of a smaller set of materials, such as microbes or even subclasses of microbes.

It should also be noted that PCA is not a cluster algorithm. Rather it is a method by which high resolution data can be compared to quickly assess which spectral regions, if any, provide chemical separation or differentiability. It should also be noted that all the separations stated here are traced back to chemistry by looking at the weightings and extrapolating the chemical nature that is driving the separation. This is described in more detail in Ref. 1.

The Level One training set was created by removing the non-bio materials from the Level Zero training set and a second analysis is done Level 1 set of eigenvectors was determined. This is shown in Fig. 8. Figure 8 shows that a focused or zoomed-in PCA space created by removing some of the environmental samples and recalculating eigenvectors gives us more separation of the biological samples. Within the "biological" category are a protein, yeast, and various bacteria. The "white" materials in Fig.8 are tyrosine (on left by itself) and lysozyme near the AAs and VOCs. The biological materials, including bacterial spores, and cells, yeasts, pollens, etc. cluster well, circled in red.

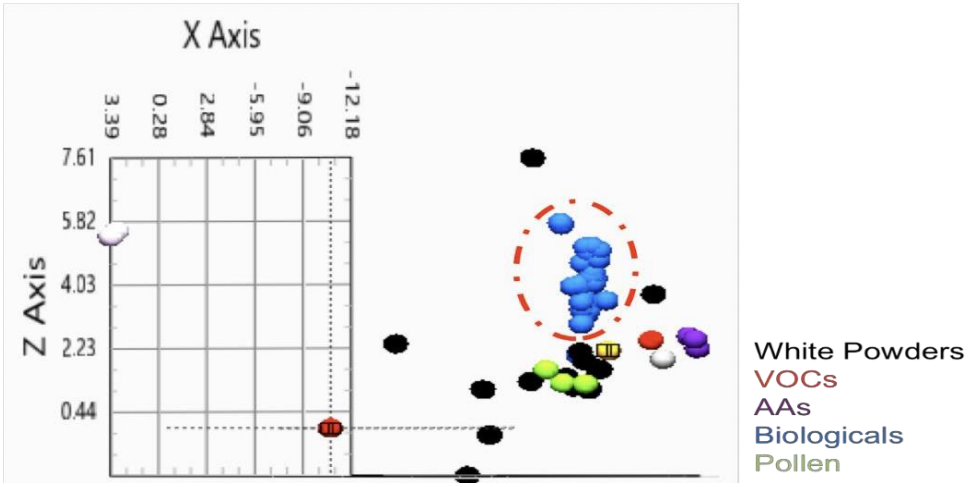

Figure 8. Level 1, "zoomed-in", PCA of bio/non-bio separation with the obviously unrelated samples removed. Ex = 248 nm.

Level 2 Analysis

The analysis for achieving Level 2 requirements is for differentiation of microbes from proteins and plant and skin cells. *This assumes that the Level 1 analysis has determined that the unknown suspicious powder is biological and is NOT non-biological.* This requires a Level Two training set for eigenvectors, which uses only biological material. This can be done automatically in a future version of BRANE sensor software. Presently, triage data analyses are being done manually. The samples used for Level 2 analysis are cleaned microbes, proteins, and plant and yeast cells. The same spectral data base from these samples was used, after determining the suspicious powder was biological, to re-train the eigenvectors for the PCA. The results are shown in Fig. 9, showing the differentiability of bacteria, proteins, and yeast.

It should be noted that while calculating a new eigenvector training set is a slow, computer intensive calculation, these calculations will not need to be performed on the instrument. It is expected that as the database of materials expands, the weights to perform these separations will be refined and calculated offboard the sensor. BRANE analysis in the field would only require the use of the training set weights for each Level. As such the calculations for this process are simple and can be performed on an embedded processor and/or a small FPGA.

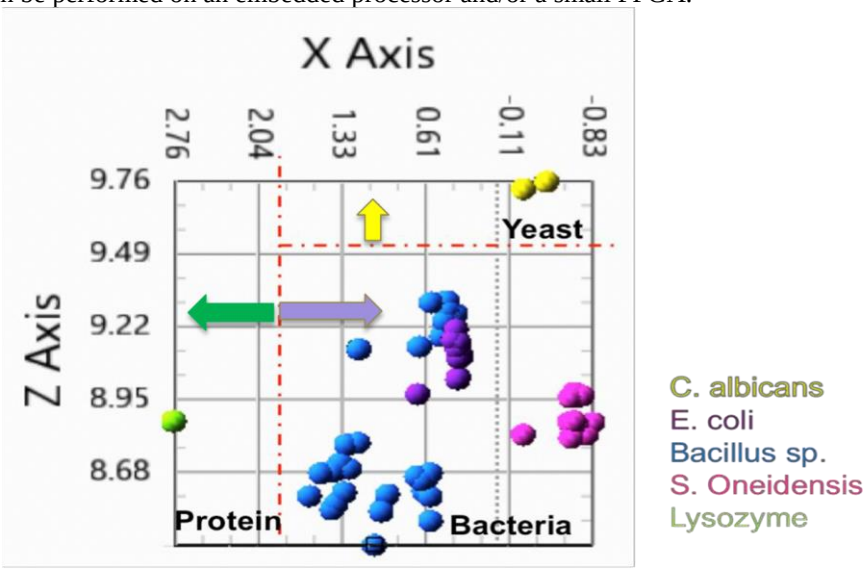

Figure 9. Triage Level 2: separation of protein from bacteria and yeast using Level 2 training set.

Level 3 Analysis

At Level 3 of specificity, the BRANE sensor needs to be able to accurately and rapidly differentiate bacterial cells, bacterial spores, yeast, fungi, and fungal spores, but proteins are removed from the training set. At Level 3, you will note in Fig. 6 that the solid lines in the triage flow diagram start to change from solid lines to dashed lines. Solid lines indicate what has been demonstrated. Dashed lines indicate what appears to be possible, but which had not yet been confirmed, until now. The present BRANE 1.0 sensor uses a 32-channel PMT array detector. The spectral coverage and resolution can be changed using different gratings. Most of the data presented above was taken with a 1200 g/mm grating, providing a dispersion or bandpass per pixel about 3.3 nm.

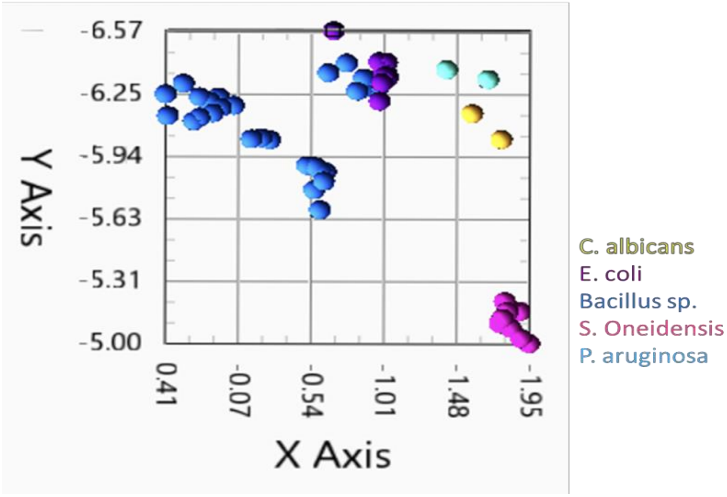

Figure 10. Triage Level 3: separation of microorganisms, bacteria, and yeast using Level 2 training set.

For the Level 3, we employed a Level 3 eigenvector training set which removed the protein in order to focus on the microorganisms and attempt further separation, as shown in Fig. 10. Figure 10 shows that microbial separation is possible using the Brane 1.0, deep UV fluorescence detection methodology. This data set does not include pure spores; however, it does include multiple species of Bacilli, which are all a mix of bacterial cells and spores.

As we require more and more specificity in classifying biological powders, we believe the requirement for higher fluorescence spectral resolution. Fortunately, for the BRANE 1.0 sensor we can easily achieve sub-1 nm bandpass simply by going to a higher dispersion grating. Nominally we can achieve 1 nm bandpass with a 3600 g/mm grating. But, for now, we are attempting to achieve a high a level of specificity with the larger 3.3 nm bandpass. Beyond that we will go to the BRANE 2.0 sensor with about 30 x smaller bandpass, or about 0.1 nm and be able to provide for Raman detection, although a much slower detection speeds with higher limits of detection.

Level 4 Analysis

At Level 4 of specificity, the BRANE sensor needs to be able to differentiate different genera of bacterial spores and cells. We used a Level 4 training set, which removes all yeasts. We have demonstrated, even with the lower fluorescence spectral resolution of the BRANE 1.0 sensor, the ability to distinguish different genera. However, even with the BRANE 1.0 sensor with 1200 g/mm grating and 3.3 nm bandpass we can achieve fairly high levels of microbial classification, as shown in Fig. 11.

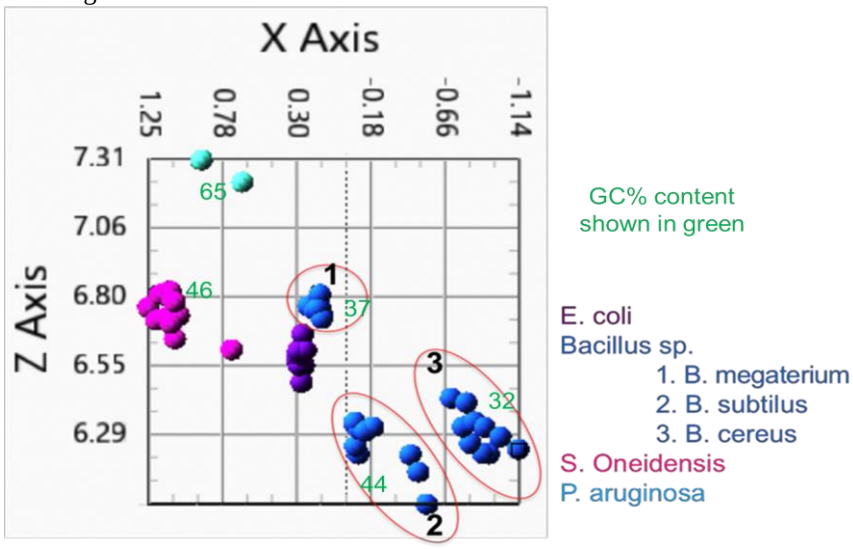

Figure 11. Triage Level 4: separation of bacteria by genus and species.

We believe the improved specificity is enabled because of the indirect relationship between Tyr/Phe content to the GC% of different bacteria. The spectrum for each microbe is unique and dependent on the ratios of tryptophan (Trp), tyrosine (Try), and phenylalanine (Phe). Furthermore, Phe and Tyr concentrations are strongly dependent on GC% content in bacterial cells [18]. This tie between Tyr and Phe with GC% content is a key component of how native fluorescence contributes to bacterial identification. Since GC% content is conserved within species but not within genera and can act as a means of taxonomic classification [19] . Two CDC Cat A bacterial cells, Y. *pestis* and F. *tularensis* have GC contents of 47% [20] and 32.9% [21] respectively. According to Lobry 1997 [18], the 15% variation in GC content would suggest that the Phe and Tyr content is higher for F. *tularensis* than Y. *pestis*. Note, that the variation in GC content for S. subtilis (44%), E. *coli* (51%) and P. *aeruginosa* (63%) are like that of F. *tularensis* than Y. *pestis* and as such show B. subtilis and E coli with an increased Tyrosine content. Some of these effects on native fluorescence spectra are shown below. We again point out that the spectra of a microorganism is not only due to its internal chemistry, but also due to the conformation and distribution of the chemistry since a complex level of fluorescence energy transfer, nearest neighbor effects, and shadowing, occur within a microorganism which give it a unique fluorescence signature, and not only its chemistry alone. It is also important to also re-iterate that excitation at a wavelength above 250 nm will cause alteration of the microbial native fluorescence emission spectra, altering the results.

A final important point is that, as early as 1993, Bronk [22] showed that the native or intrinsic fluorescence spectrum of a wide range of microbes was relatively invariant to position in a life cycle. Many of the early papers employed excitation between 270 nm to 290 nm, where strong Raman emission from the O-H stretch region of wet or water suspended microbes provided significant alteration of the native fluorescence emission of the microbes, which alter the ability to identify. Therefore, excitation below 250 nm is mandatory to employ this native fluorescence method. We have, additionally, studied the effect of cell cycle on the chemical differentiability of microbes using deep UV native fluorescence, and have concluded that as long as excitation is below 250 nm, these spectra show substantial differentiability between microbial types, independent of the position in the cell cycle. The data and clusters for individual microbial classes in Fig. 11 represent a wide range of sample preparations and concentrations from bulk to 1:70,000 dilutions and show the robustness of the method.

3. DEEP UV RAMAN & FLUORESCENCE INSTRUMENTS

The advantages of deep UV Raman spectroscopy alone and in combination with fluorescence spectroscopy have been demonstrated in many laboratory environments using large laboratory instruments. We do not provide an extensive literature here, but some literature is in the attached references. One of our goals is to bring this technology to hand-held field operations with standoff distances from a few cm to 25 m. The focus of the data shown below will be for these miniature instruments, starting with a Targeted Ultraviolet CBE (TUCBE) chemical sensor and finishing with a next generation sensor with much higher spectral resolution for both Raman and fluorescence. We will also show some results on our laboratory based macroscopic chemical mapping instruments called MOSAIC instruments with a sensitivity to a single bacterial spore or ng/cm^2 of chemical, and microscopic chemical imaging instruments with sensitivity to a small fraction of the contents of a single bacterial spore. A selection of these instruments is shown below in Table III below

Table III. Deep UV Raman & fluorescence instruments over a wide range of spatial scales.

			
	Microscopic (µMOSAIC)	Macroscopic (MOSAIC)	Standoff SHCBE, etc.
Working distance	1-10 mm	2-20 cm	1-25 m
Spatial resolution	0.2-1 µm	50-500 µm	1-10 mm
LOD	Small fraction of a single spore	Single spore or ng/cm^2 at 5 cm	60 spores or low µg per cm^2 at 5 m

Figure 5 is an example of the capability of the micro-MOSAIC instrument, shown in Table III above, where the ability to chemically image small fractions of single microbial cells is illustrated. Another deep UV instrument, the MOSAIC instrument illustrated in Table III, is used to generate chemical images of much wider areas and is useful to determine the spatial distribution of trace levels of chemical, microbial, and explosives on surfaces, down to the single bacterial spore or ng/cm2 level. This has also been used for reagentless fingerprint detection of a wide range of surfaces, as well as to determine the distribution of microparticle in-fall on surfaces left for months at a time including microbes, pollens, etc. It is also used for mapping the distribution and concentration of chemicals in Antarctica ice cores, where deep UV penetration is many cm in these ice cores. An illustration is shown below in Fig. 12 of reagentless fingerprint detection of a wide range of materials, including identification of chemicals imbedded in the fingerprints, and fingerprints on a bullet.

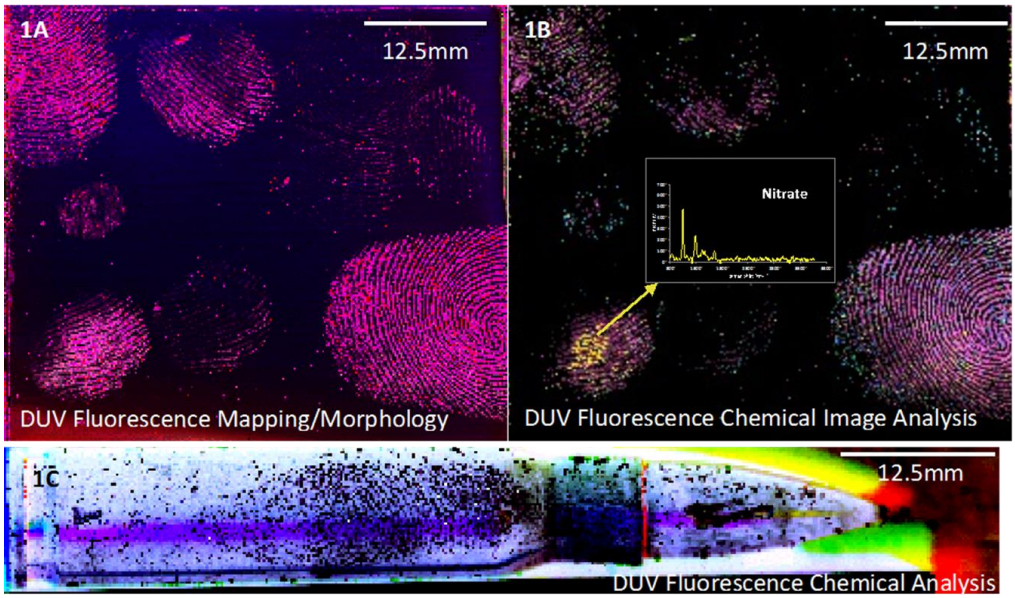

Figure 12. Illustrations of reagentless fingerprint and chemical analysis using deep UV methods with the Photon Systems MOSAIC system.

A further example of deep UV detection is the ability to measure the distribution of microbial material on a standard painted wall at 6 m standoff, using a predecessor instrument to the SHCBE instrument illustrated in Table III in Fig. 13 below.

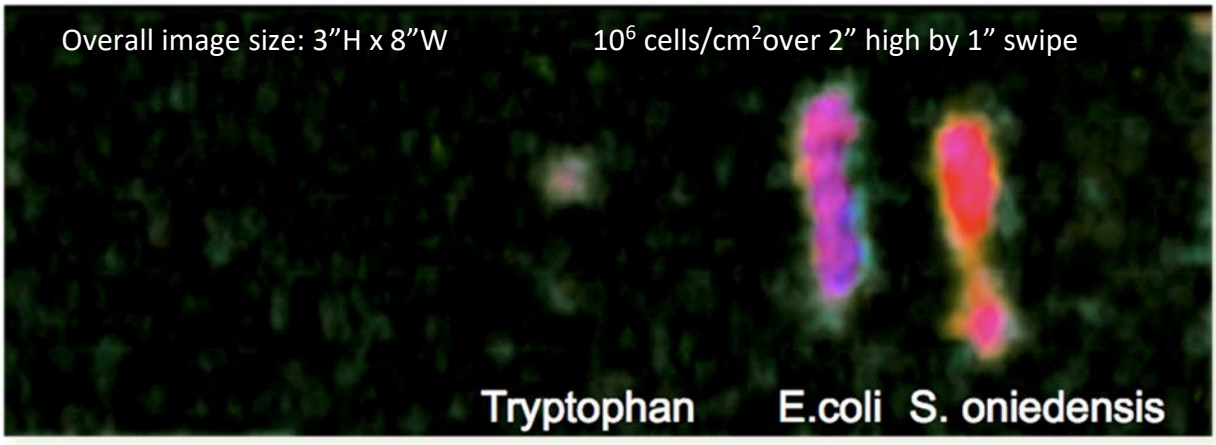

Figure 13. Illustration of 6 m standoff detection of trace microbial concentrations on an off-white painted wall. Microbial colors use a UV to visible RGB color translation. Traces of these microbes were still present after washing the wall with alcohol.

4. SUMMARY

We have demonstrated the ability to detect and classify trace concentrations of microbial material embedded in a host of common interferents or confusants, without contact or sample handling. Detection occurs in factions of a second at rates of up to about 20 detections per second and at standoff distance from 5 cm to 5 m without any interference from natural or manmade sources of light.

The method employs deep UV fluorescence spectroscopy with excitation below 250 nm to separate the spectral regions of both fluorescence and Raman emissions. This ensures that the complete fluorescence spectral range of microbes is detected without any spectral alteration due to overlap with strong OH stretch Raman bands of water within the sample or within the laser beam spot on a targeted area. Spectral separation also enables Raman spectra to be detectable with no fluorescence interference or obscuration. Excitation at wavelengths above 250 nm from, as an example, a 262 nm or 266 nm laser, will cause alteration of the fluorescence spectra of microbes in the 280 nm to 320 nm spectral range, which alters the results and makes microbial classification difficult or impossible.

The method is reagentless and non-destructive and provides detection without precluding the potential to use other methods for confirmation of findings, such as PCR. The method demonstrated is, effectively, a high-level trigger instrument to warn of possible hazardous chemical, biological, or explosive material on surfaces within the standoff range of the sensor.

This paper also illustrates new deep UV hand-held and laboratory analytical sensors and instruments that cover a wide range of spatial scales from about 400 nm to 1 cm and enable detection of CBE materials at a range of standoff distances from a few cm up to 5 m and more, with low limits of detection.

5. ACKNOWLEDGEMENTS

Photon Systems gratefully acknowledges the support of: U.S. Army SBIR Contract No. W911NF-14-C-0142 and DTRA Contract No. HDTRA1-17-C-0016.

6. REFERENCES

[1] Hug, W.F., R. Bhartia, K. Sijapati, L.W. Beegle, and R.D. Reid, "Improved sensing using simultaneous deep UV Raman and fluorescence detection-II", SPIE Security & Defense, SPIE Security & Defense, Vol. 9073, No. 20, 7 May (2014).

[2] Asher, S.A., and C.R. Johnson, "Raman Spectroscopy of a Coal Liquid Shows That Fluorescence Interference Is Minimized with Ultraviolet Excitation", Science, 225, 311-313, 20 July (1984).

[3] Asher, S.A. and C.R. Johnson, "UV Resonance Raman Excitation Profile Through the $^1B_2$ State of Benzene", J. Phys. Chem. Vol. 89, pp. 1375-1379 (1985).

[4] Sparrow, M.C., J.F. Jackovitz, C.H. Munro, W.F. Hug, and S.A. Asher, "A New 224nm Hollow Cathode UV Laser Raman Spectrometer", J. App. Spectroscopy, Vol. 55, No. 1, Jan 2001.

[5] Storrie-Lombardi, M. C., W. F. Hug, G. D. McDonald, A. I. Tsapin, and K. H. Nealson. "Hollow cathode ion laser for deep ultraviolet Raman spectroscopy and fluorescence imaging". Rev. Sci. Instruments, Vol. 72, No.12, pp.4452-4459, Dec. 2001.

[6] Hug, W.F., R. Bhartia, A. Tsapin, A.L. Lane, P. G. Conrad, K. Sijapati, and R.D. Reid, "Status of miniature integrated UV resonance fluorescence and Raman sensors for detection and identification of biochemical warfare agents", Proc. SPIE, Vol. 5994, Boston, MA., Oct. 22-26, 2005.

[7] A new miniature, hand-held, solar-blind, reagentless standoff chemical, biological, and explosives (CBE) sensor", Proc. SPIE/Security & Defense, Vol. 6954, No.17, Orlando, FL., March 19, 2008.

[8] Bhartia, R., W.F. Hug, E. Salas, R. Reid, K. Sijapati, A. Tsapin, W. Abbey, P. Conrad, K. Nealson, and A. Lane. "Classification of organic and biological materials with deep UV excitation". Applied Spectroscopy, Vol. 62, No. 10, October 2008.

[9] Hug, W. F., R.D. Reid, R. Bhartia, and A.L. Lane, "Performance Status of a Small Robot-Mounted or Hand-Held Solar Blind Standoff Chemical, Biological and Explosives Sensor", SPIE Security & Defence, Vol. 7304, No. 36, April 15, 2009.

[10] Bhartia,R., E.C. Salas, W.F. Hug, R.D. Reid, A.L. Lane, K.J. Edwards, and K.J. Nealson, "Label-free bacterial imaging with deep UV laser induced native fluorescence", Applied and Environmental Microbiology, Vol. 76, No. 21, pp. 7231-7237, Nov. 2010.
[11] Beegle, L.W., R. Bhartia, W. Hug, et.al., "SHERLOC: Scanning Habitable Environments with Raman and Luminescence for Organics and Chemicals", 45th Lunar & Planetary Science Conference, p. 2835, Houston, TX, 2014
[12] Salas, E. C., R. Bhartia, L. Anderson, W.F. Hug, R.D. Reid, G. Iturrino, & K.J. Edwards, "In situ detection of microbial life in the deep biosphere in igneous ocean crust", Frontiers in Microbiology- Extreme Microbiology. 15 November 2015.
[13] Abbey, W.J., R. Bhartia, L. Beegle, L. DeFlores, V. Paez, K. Sijapati, S. Sijapati, K. Williford, M. Tuite, W. Hug, and R. Reid, "Deep UV Raman spectroscopy for planetary explorations: The search for in situ organics", Icarus Elsevier, pp. 201-214, (2017)
[14] Sohn, M, et.al, "Fluorescence spectroscopy for rapid detection and classification of bacterial pathogens", Appl. Spec. V 63, 11, pp1251-5, Nov. (2009).
[15] Dartnell, L.R., et.al., "Fluorescence characterization of clinically-important bacteria", PLOS One, 30 Sept. (2013).
[16] Walsh, J.D., et.al., "Rapid intrinsic fluorescence method for direct identification of pathogens in blood cultures", Am Soc. For Microbiology,
[17] Madigan, M.T., et.al, Brock Biology of Microorganisms p 991, (2000).
[18] Lobry, J.R., "Influence of genomic G+C content on average amino-acid composition of proteins from 59 bacterial species", Gene 205 (1997), pp 309-316.
[19] Wayne, L G, D J Brenner, R R Colwell, PAD Grimont, O Kandler, M I Krichevsky, L H Moore, WEC Moore, RGE Murray, and E. Stackebrandt. 1987. "Report of the ad hoc committee on reconciliation of approaches to bacterial systematics." International Journal of Systematic Bacteriology 37(4): 463–464.
[20] Perry, R D, and J D Fetherston. 1997. "Yersinia pestis--etiologic agent of plague." Clinical microbiology reviews 10(1): 35–66.
[21] Larsson, Pär, Petra C F Oyston, Patrick Chain, May C Chu, Melanie Duffield, Hans-Henrik Fuxelius, Emilio Garcia, Greger Hälltorp, Daniel Johansson, Karen E Isherwood, Peter D Karp, Eva Larsson, Ying Liu, Stephen Michell, Joann Prior, Richard Prior, Stephanie Malfatti, Anders Sjöstedt, Kerstin Svensson, Nick Thompson, Lisa Vergez, Jonathan K Wagg, Brendan W Wren, Luther E Lindler, Siv G E Andersson, Mats Forsman, and Richard W Titball. 2005. "The complete genome sequence of Francisella tularensis, the causative agent of tularemia." *Nature Genetics* 37(2): 153–159.
[22] Bronk, B.V., L. Reinisch, "Variability of Steady-State Bacterial Fluorescence with Respect to Growth Conditions", App. Spect., V 47, No. 4, 1993.